AFRL-RW-EG-TP-2014-005

Annular Pulse Shaping Technique for Large-Diameter Kolsky Bar Experiments on Concrete

Bradley E. Martin
Air Force Research Laboratory, Munitions Directorate
AFRL/RWMW
101 W. Eglin Blvd., Ste 135
Eglin AFB, FL 32542

William F. Heard, Thomas Slawson
U.S. Army Engineer Research and Development Center
Vicksburg, MS 39180

Xu Nie
Department of Mechanical and Energy Engineering
University of North Texas
Denton, TX 76203

P. K. Basu
Department of Civil and Environmental Engineering
Vanderbilt University
Nashville, TN 37240

OCTOBER 2014

INTERIM REPORT

AIR FORCE RESEARCH LABORATORY
MUNITIONS DIRECTORATE
■ **Air Force Materiel Command** ■ **United States Air Force** ■ **Eglin Air Force Base, FL 32542**

NOTICE AND SIGNATURE PAGE

Using Government drawings, specifications, or other data included in this document for any purpose other than Government procurement does not in any way obligate the U.S. Government. The fact that the Government formulated or supplied the drawings, specifications, or other data does not license the holder or any other person or corporation; or convey any rights or permission to manufacture, use, or sell any patented invention that may relate to them.

Qualified requestors may obtain copies of this report from the Defense Technical Information Center (DTIC) <http://www.dtic.mil/dtic/index.html>.
.

AFRL-RW-EG-TP-005 HAS BEEN REVIEWED AND IS APPROVED FOR PUBLICATION IN ACCORDANCE WITH ASSIGNED DISTRIBUTION STATEMENT.

FOR THE DIRECTOR:

DAVID E. LAMBERT
Ordnance Sciences CTC Lead, Ordnance Division

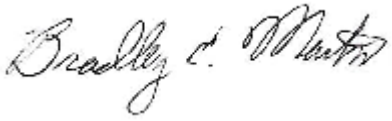

BRADLEY E. MARTIN
Program Manager, Damage Mechanisms Branch

MATT J. MATYAC
Technical Advisor, Damage Mechanisms Branch

This report is published in the interest of scientific and technical information exchange, and its publication does not constitute the Government's approval or disapproval of its ideas or findings.

REPORT DOCUMENTATION PAGE

Form Approved
OMB No. 0704-0188

1. REPORT DATE *(DD-MM-YYYY)*	2. REPORT TYPE	3. DATES COVERED *(From - To)*
13-6-2014	Technical Publication	October 2012 - February 2014

4. TITLE AND SUBTITLE

ANNULAR PULSE SHAPING TECHNIQUE FOR LARGE-DIAMETER KOLSKY BAR EXPERIMENTS ON CONCRETE

5a. CONTRACT NUMBER
N/A

5b. GRANT NUMBER
N/A

5c. PROGRAM ELEMENT NUMBER

6. AUTHOR(S)
(1) Bradley E. Martin, RWMW
(2) William F. Heard, Engineer Research and Development Center
(3) Thomas Slawson, Engineer Research and Development Center
(4) Xu Nie, University of North Texas
(5) P.K. Basu, Vanderbilt University

5d. PROJECT NUMBER
2502

5e. TASK NUMBER
9210

5f. WORK UNIT NUMBER
W0DT

7. PERFORMING ORGANIZATION NAME(S) AND ADDRESS(ES)
(2)(3) U.S. Army Engineer Research and Development Center,Vicksburg, MS 39180
(4) Department of Mechanical and Energy Engineering, University of North Texas Denton, TX 76203
(5) Department of Civil and Environmental Engineering, Vanderbilt University

8. PERFORMING ORGANIZATION REPORT NUMBER
AFRL-RW-EG-TP-2014-005

9. SPONSORING/MONITORING AGENCY NAME(S) AND ADDRESS(ES)
(1) Air Force Research Laboratory, Munitions Directorate, AFRL/RWMW, 101 West Eglin Blvd., Eglin AFB, FL 32542

10. SPONSOR/MONITOR'S ACRONYM(S)
AFRL/RWMW

11. SPONSOR/MONITOR'S REPORT NUMBER(S)
Same as block 8

12. DISTRIBUTION/AVAILABILITY STATEMENT

DISTRIBUTION A. Approved for public release: distribution unlimited (PA# 96TW-2014-0048)

13. SUPPLEMENTARY NOTES

14. ABSTRACT

The goal of this study is to design a novel annular pulse shaping technique for large-diameter Kolsky bars for investigating the dynamic compressive response of concretes. The purpose of implementing an annular pulse shaper design is to alleviate inertia-induced stresses in the pulse shaper material that would otherwise superpose unwanted oscillations on the incident wave. This newly developed pulse shaping technique led to well-controlled testing conditions enabling dynamic stress equilibrium, uniform deformation, and constant strain-rate in the testing of a chosen concrete material. The observed dynamic deformation rate of the concrete is highly consistent (8 % variation) with the stress in the specimen well equilibrated confirming the validity of this new technique. Experimental results at both quasi-static and dynamic (100/s, 240/s) strain rates showed that the failure strength of this concrete is rate-sensitive.

15. SUBJECT TERMS

Split-Hopkinson Pressure Bar, Pulse shaper, High strength concrete, High rate, Large Kolsky bar

16. SECURITY CLASSIFICATION OF:			17. LIMITATION OF ABSTRACT	18. NUMBER OF PAGES	19a. NAME OF RESPONSIBLE PERSON
a. REPORT	b. ABSTRACT	c. THIS PAGE			Bradley E. Martin
UNCLAS	UNCLAS	UNCLAS	SAR	16	19b. TELEPHONE NUMBER *(Include area code)* (850)882-6776

Experimental Mechanics (2014) 54:1343–1354
DOI 10.1007/s11340-014-9899-6

Annular Pulse Shaping Technique for Large-Diameter Kolsky Bar Experiments on Concrete

W.F. Heard · B.E. Martin · X. Nie · T. Slawson · P.K. Basu

Received: 11 February 2014 / Accepted: 30 April 2014 / Published online: 13 June 2014

Abstract The goal of this study is to design a novel annular pulse shaping technique for large-diameter Kolsky bars for investigating the dynamic compressive response of concretes. The purpose of implementing an annular pulse shaper design is to alleviate inertia-induced stresses in the pulse shaper material that would otherwise superpose unwanted oscillations on the incident wave. This newly developed pulse shaping technique led to well-controlled testing conditions enabling dynamic stress equilibrium, uniform deformation, and constant strain-rate in the testing of a chosen concrete material. The observed dynamic deformation rate of the concrete is highly consistent (8 % variation) with the stress in the specimen well equilibrated confirming the validity of this new technique. Experimental results at both quasi-static (10^{-4} s^{-1}) and dynamic (100 s^{-1}, 240 s^{-1}) strain rates showed that the failure strength of this concrete is rate-sensitive.

Keywords Split-hopkinson pressure bar · Pulse shaper · High strength concrete · High rate · Large kolsky bar

W.F. Heard · T. Slawson
U.S. Army Engineer Research and Development Center, 39180 Vicksburg, MS, USA

W.F. Heard
e-mail: William.F.Heard@usace.army.mil

B.E. Martin (✉)
Air Force Research Laboratory, 32542 Eglin AFB, FL, USA
e-mail: bradley.martin@eglin.af.mil

X. Nie
Department of Mechanical and Energy Engineering, University of North Texas, 76203 Denton, TX, USA
e-mail: Xu.Nie@unt.edu

P.K. Basu
Department of Civil and Environmental Engineering, Vanderbilt University Nashville, 37240 Nashville, TN, USA
e-mail: p.k.basu@vanderbilt.edu

Introduction

In the past two decades, the quest of exploring the dynamic response of concrete-like materials has reached a common consensus that above a certain transitional strain-rate, the strength of concrete is highly dependent on strain-rate. This dependency is often described by the Dynamic Increase Factor (DIF), which is defined as the ratio between the dynamic and quasi-static strength with increasing strain-rate under uniaxial compressive and tensile loading conditions. From the materials perspective, a few theories have been developed to explain the published results either by the generation, dynamic growth, and interaction of sliding micro cracks [34], or by the viscoelastic nature of the cement material as well as the time-dependent crack growth [16]. Other studies, however, tend to attribute the observed strength increase to the artifacts inherent in the physical architecture of the high-rate experimental techniques. For example, the friction effect between the specimen and bars in Kolsky bar experiments may enhance the compressive strength of concrete. This effect has been proven to be strain-rate sensitive [29, 32]. Furthermore, the radial inertia in the specimen, due to axial strain-rate acceleration, is believed to impose an artificial radial confining stress to the concrete and may contribute to the enhanced dynamic strength [21, 50].

Despite ongoing debates on the true mechanisms causing the strain-rate effects in concrete, experimentalists continued to improve the high-rate Kolsky bar characterization techniques for brittle materials in hope to interpret the experimental results on concrete with higher accuracy and less uncertainty. A technique commonly used in Kolsky bar experiments to facilitate proper loading of the specimen material is the pulse shaping technique which was originally developed by Duffy et al. [17] in Split-Hopkinson torsion bar experiments on Aluminum. The work by Duffy et al. placed thin strips of lead between the striker bar and torsional bar while a short

piece of tubing, called a "pulse smoother", was placed between the torsional bar and specimen. The pulse shaping technique was further expanded upon by Ellwood et al. [18] by incorporating "dummy" specimens, of the same material as the specimen, and placing it between the striker and pre-loading bar to provide pulse shaping of the loading wave. The technique of Ellwood et al. was later modified by Parry et al. [40] by removing the "dummy" specimen and using only the pre-loading bar between the striker and incident bar. To increase the utility of the pulse shaping technique the typical right-circular cylinder striker bar was replaced with striker bars that used varying truncated cone and spherical cap geometries to create the desired loading wave [13, 22]. The second pulse shaping technique presented by Frantz et al. [22] used traditional right-circular cylinder striker bars but placed thin pieces of varying materials between the striker bar and incident bar and is the common technique used in the Kolsky bar research community. These pioneering efforts primarily focused on characterization of ductile materials.

For brittle materials, Nemat-Nasser et al. [35] suggested applying a thin piece of metal on the impact end of the incident bar in the Kolsky bar experiment to facilitate a linear-ramp loading wave profile so that well-defined boundary conditions (i.e., dynamic stress equilibrium, constant strain-rate and deformation) may be achieved in the specimen. This pulse shaping concept was further developed by Frew et al. [23, 24] to specifically address the dynamic testing of geomaterials. The analytical/experimental results reported by Frew et al. [23, 24] have shown that in order to realize constant strain-rate deformation in Kolsky compression bar experiments of brittle materials, it is essential to generate a linear incident loading wave by choosing the proper combination of pulse shaper dimensions and striker bar impact velocity. Considering the widely-observed rate sensitivity of concrete, constant strain-rate deformation prior to specimen failure is a critical experimental condition. During constant strain-rate deformation the axial strain-rate acceleration becomes zero and therefore reduces the inertia induced confining stress on the specimen [21]. The absence of the inertia effects significantly simplifies the interpretation of failure strength by ensuring the desired uniaxial stress state in the specimen (except during the early stage of deformation where the strain-rate increases from zero to a constant level). Simultaneously, the linear incident pulse facilitates dynamic stress equilibrium to ensure uniform deformation of the specimen while preventing premature failure [23, 24, 35]. This concept has been successfully practiced by a number of Kolsky bar researchers on a variety of brittle materials such as glass, ceramics, and ceramic composites using relatively small specimen geometries [12, 28, 36, 38, 45]. However, due to the large aggregate size and inhomogeneous void distribution in concrete materials it is desirable to adopt larger specimens with a representative volume of the constituent materials in order to limit the variation of experimental results. This led to the need for large-diameter Kolsky bars that have been extensively used in previous high-rate studies on concrete materials [1, 6, 7, 10, 20, 41–43]. As previously reported in the literature [6, 7, 16, 29, 32, 41–43], the mechanical properties of concrete materials are sensitive to the deformation rate and many factors exist, intrinsic to the material or not, that can contribute to the rate sensitivity. From an experimental point of view, it is critical to develop a reliable high-rate experimental technique to accommodate large specimen geometries while acquiring similar specimen boundary conditions (i.e., dynamic stress equilibrium, constant strain-rate and deformation) rationalized in small-diameter Kolsky bar experiments on brittle materials.

The recent progress in developing such characterization capabilities for concretes at the High-Pressure Particulate Physics (HP3) Facility, U.S. Air Force Research Laboratory, Eglin AFB, FL is reported herein. The study is centered on establishing a reliable pulse shaping technique for characterizing concretes using large-diameter Kolsky bars. If a linearly scaled-up solid pulse shaper design is adopted from smaller Kolsky bars [23, 24], the radial inertia in the pulse shapers superposes noise-like oscillations on the incident wave. This type of interference significantly compromises the targeted linear incident wave profile desired for brittle materials characterization. The proposed new approach specifically addresses this issue by introducing the concept of an annular pulse shaper. High strain-rate compression results on a Self-Consolidating High-Strength Concrete (SCHSC) showed that the annulus pulse shaping technique effectively reduces the radial inertia effects in the pulse shapers while allowing both constant strain-rate deformation and dynamic stress equilibrium to be achieved in the specimens to ensure valid testing conditions.

Kolsky Compression Bar Experiments

Material Properties

A SCHSC was selected for the present study. Self-consolidating concrete is a highly flowable and non-segregating concrete that can spread into tight and constricted spaces under gravity without the need for vibrating compaction. Characteristics of high-flow and high-strength are not typically both achieved in a cementitious material. However, SCHSC was developed with a 3rd-generation High-Range Water Reducing Admixture (HRWRA) and a Viscosity Modifying Admixture (VMA) to optimize the material rheology and mechanical properties. Table 1 shows the mixture proportions (by weight) for the SCHSC. Constituent proportions are shown relative to the total amount of cementitious material (CM), which is comprised of ASTM type I/II cement [2], Grade 120 Slag cement [5] and Class F fly ash [4]. The

Table 1 Mix Proportions for the SCHSC Material

Constituent	Mix proportions (by weight of total CM)[a]
Cement	0.70
Slag cement	0.15
Fly ash	0.15
Aggregate	1.30
VMA	0.006
HRWRA	0.0128
Water	0.37

[a] CM (total cementitious material) = cement + slag cement + fly ash

gradation analysis results for the SCHSC aggregate are shown in Table 2.

Specimen Fabrication

All specimens were fabricated from an Self-Consolidating High-Srength Concrete (SCHSC) developed by the U.S. Army Engineer Research and Development Center, Vicksburg, MS. The material was placed in steel tubs and allowed to cure for 91 days in a temperature controlled lime-water bath at 23 °C (as per ASTM C192 [3]) prior to specimen fabrication to ensure the desired unconfined compressive strength of approximately 80 MPa (12 ksi) was acquired. Following material curing, several 50.8 mm cores were drilled from the tubs using a core drill system and then carefully sectioned, using a Beuhler Delta-EB 260 manual abrasive cutter, to yield multiple SCHSC disks with an approximate thickness of 19.05 mm. It should be noted that the brittleness of concrete introduces significant challenges for Kolsky bar testing and it is critical to fabricate specimens with flat and parallel face ends to ensure uniform loading. To ensure the best quality regarding specimen parallelism and flatness a two-stage process was used.

In the first stage, the initial rough thickness was reduced from 19.05 to 13.97 mm while ensuring maximum possible parallelism by removing material from each face with a precision Harig 618 Auto step surface grinder. Once all the disks were surfaced, they were placed in a high precision P.R. Hoffman PR-1 double-sided lapping machine to obtain final parallelism, flatness, and specimen thickness of 12.7 mm. The finished specimens were then weighed along with specimen diameter and thickness measurements to calculate specimen density. Specimen properties are given in Table 3.

Table 2 Gradation analysis of aggregate used in SCHSC

Sieve size (mm)	Passing (%)
#10 (2.00)	100.0
#16 (1.18)	98.8
#20 (0.85)	87.2
#30 (0.600)	57.8
#40 (0.425)	45.2
#50 (0.300)	37.7
#70 (0.212)	31.4
#100 (0.150)	26.6
#140 (0.106)	22.9
#200 (0.075)	20.3

Kolsky Compression Bar Theory and Setup

Kolsky bar, also known as Split-Hopkinson Pressure Bar (SHPB), is an instrumented device for testing the high strain-rate response of materials under uniaxial dynamic stress loading conditions [30]. The technique is based on one-dimensional stress wave theory in elastic solids. The schematic of a typical Kolsky compression bar setup is shown in Fig. 1.

In general, the gas-gun-driven striker bar impacts one end of the incident bar (through proper pulse shaping) to generate an incident wave that travels to the other end, where the specimen is located, and loads the specimen at high strain-rates. Due to the difference in mechanical impedance between the bar material and specimen, part of the input energy is reflected back into the incident bar from the loaded specimen while the remaining energy is transmitted through the specimen and into the transmission bar. Strain gages mounted on the incident and transmission bar surfaces collect the wave histories that are subsequently used to calculate the specimen stress and strain. The theory of the Kolsky bar technique has been extensively documented (see Gray [26]) and will only be briefly presented herein. The specimen stress and strain are given by equations 1 and 2.

$$\varepsilon(t) = \frac{2C_0}{L_s}\int_0^t \varepsilon_r(t)dt \tag{1}$$

$$\sigma(t) = E_b\frac{A_b}{A_s}\varepsilon_t(t) \tag{2}$$

In equations 1 and 2, $\varepsilon(t)$ is the specimen strain history, $\sigma(t)$ the specimen stress history, ε_r the reflected strain, ε_t the

Table 3 Properties for SCHSC Specimens

Density	Diameter[a]	Thickness[a]
(kg/m^3)	Mean (3SD)[b]	Mean (3SD)
2.113 (0.102)	50.575 (0.489)	12.223 (0.555)

[a] All dimensions are in (mm)

[b] 3 Standard Deviations (3SD)

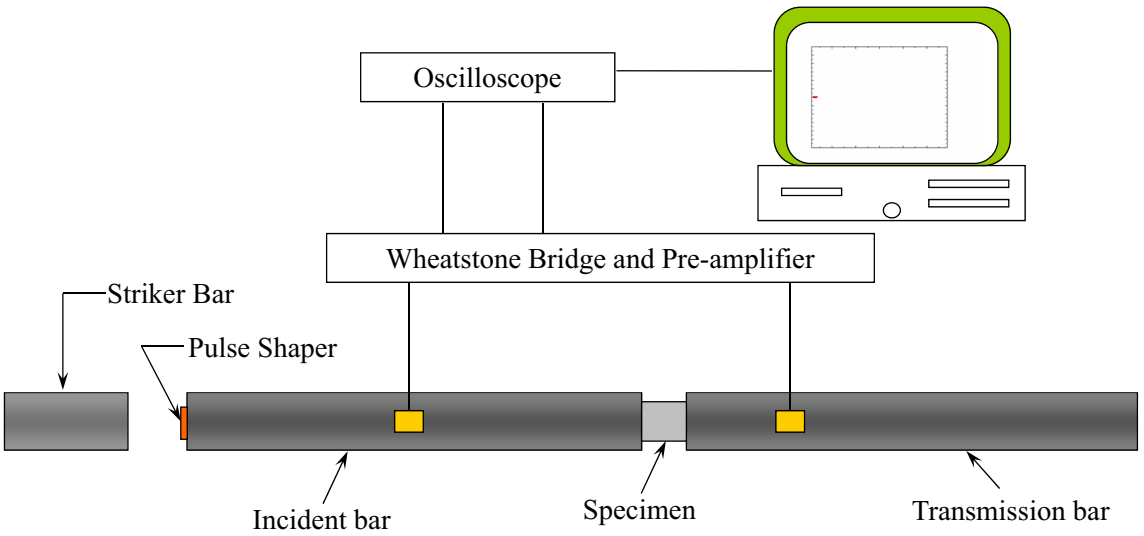

Fig. 1 Schematic of a typical Kolsky compression bar setup

transmitted strain, A_b the bar cross-sectional area, A_s the initial specimen cross-sectional area, and L_s the initial specimen length. In equation 1, C_0 is the one-dimensional stress wave velocity and E_b the Young's Modulus of the bar material. In this study, the striker, incident, and transmission bars were 50.8 mm in diameter and fabricated from PH 13–8 Molybdenum stainless steel bars with a Young's Modulus, E_b = 221 GPa, yield strength, σ_y = 1.415 GPa, and bar wave velocity, C_0 = 5,104 ms^{-1}. The lengths of incident and transmission bars are 3.66 and 3.35 m, respectively. In an effort to significantly minimize friction a high-pressure MoS_2 paste lubricant was applied at the specimen-bar interfaces in all experiments. Considering the large size and weight of the bars, linear air bushings were incorporated at all mounting locations in lieu of conventional brass bearings to reduce friction to the bars while in motion (see Fig. 2(b)). The general arrangement of the 50.8 mm Kolsky bar was presented in Fig. 1 with photos of the Kolsky bar used for this study presented in Fig. 2.

Pulse Shaping Technique

Radial Inertia in Pulse Shapers

The Kolsky bar pulse shaping technique for brittle materials has been evolving over the past two decades [11, 12, 23, 24, 28, 35, 36, 38, 45]. The effectiveness of applying this technique to test different materials is contingent on acquiring dynamic stress equilibrium and specimen deformation under constant strain-rate. The former ensures a uniform stress distribution in the specimen along the loading direction to obtain uniform deformation while the latter is regarded as the common practice for mechanical characterization of most, if not all, materials under uniaxial loading conditions. To satisfy these two criteria in Kolsky bar experiments on brittle materials, a linear loading wave is desired considering the linear elastic nature of such materials [24].

A linear loading wave can be realized with good repeatability by using a solid annealed copper disk pulse shaper.

(a) (b)

Fig. 2 Photographs of the 50.8 mm Kolsky bar: (**a**) Kolsky bar arrangement; (**b**) air bushing and mount

Examples of successful application of this technique were reported in many studies [12, 28, 36, 38, 45] using relatively small-diameter Kolsky bars (<20 mm diameter). One common characteristic for many concretes is that the material exhibits substantial heterogeneity due to the presence of various types of large-size constituents (e.g. steel fibers, air voids, aggregate, etc.). To minimize variability in experimental data and to have a representative specimen volume, due to heterogeneities, large specimen geometries are desired for mechanical characterization. Therefore, to accommodate larger specimen geometries the diameter of the Kolsky bars also needs to be increased. In designing the pulse shaper for large-diameter Kolsky bars one approach is to apply what has been established for small-diameter Kolsky bars by linearly scaling the diameter of the small pulse shapers proportionally with the bar diameters. This approach is intuitive since small pulse shapers have been proven to produce the desired linear loading wave for brittle materials [36].

Implementing this concept the incident waveform obtained using a large solid copper pulse shaper, 25.4 mm in diameter and 1.5 mm thick, on the 50.8 mm Kolsky compression bar is shown in Fig. 3(a). The pulse shaper dimensions and striker bar impact velocity were carefully designed from smaller Kolsky bar experiments on brittle materials.

Figure 3(a) shows that the incident wave does not exhibit a triangular waveform but instead shows that oscillations exist within the waveform throughout the entire loading event. To investigate whether the oscillations were introduced by the experimental setup, the pulse shaper diameter was reduced to 9 mm corresponding to the more common pulse shapers previously used in the literature [36]. The resulting incident waveform is shown in Fig. 3(b). It is clear that the expected linear incident wave was not generated due to the much smaller pulse shaper diameter in comparison to the 50.8 mm diameter Kolsky bar. No oscillations were observed in this waveform as compared to the waveform in Figure 3(a). Based on the differences shown between Fig. 3(a) and (b), it was concluded that the undesired oscillations in the incident waveform resulted from increasing the pulse shaper diameter. To obtain quantitative deformation information for the pulse shaper a 25.4 mm diameter by 1.5 mm thick pulse shaper was placed in the specimen gage section between the incident and transmission bars. The purpose of treating the pulse shaper as a specimen was to record the stress (transmitted wave) and strain-rate (reflected wave) histories for analysis. The pulse shaper specimen was subsequently loaded by an incident wave generated by the impact of the striker bar without the use of pulse shapers at the incident/striker bar interface. The correlated specimen stress and strain-rate histories are presented in Fig. 4. Figure 4 shows that the specimen strain-rate is not constant but triangular in shape with distinctive acceleration and deceleration slopes. The region around the peak of the strain-rate history corresponds to the peak-to-valley decrease in stress (from "a" to "b") in the specimen stress history. These indicators may suggest a new hypothesis related to the effect of inertia in pulse shapers that, to the authors' best knowledge, has not yet been reported in the literature regarding pulse shaper design.

The specimen inertia effect in Kolsky compression bar experiments has been studied by several authors including Kolsky himself [8, 14, 15, 21, 25, 30, 44, 49, 50]. There are two primary sources that can generate inertia. The first comes from acceleration of the specimen strain-rate during the initial loading process where the specimen strain-rate increases from zero to a constant strain-rate. As the axial strain-rate increases the specimen radial expansion rate also accelerates requiring an additional force to overcome the inertia. The additional force presents itself in the form of a radial confining effect and inducing an additional stress component, in the axial direction, affecting the intrinsic material constitutive response. The

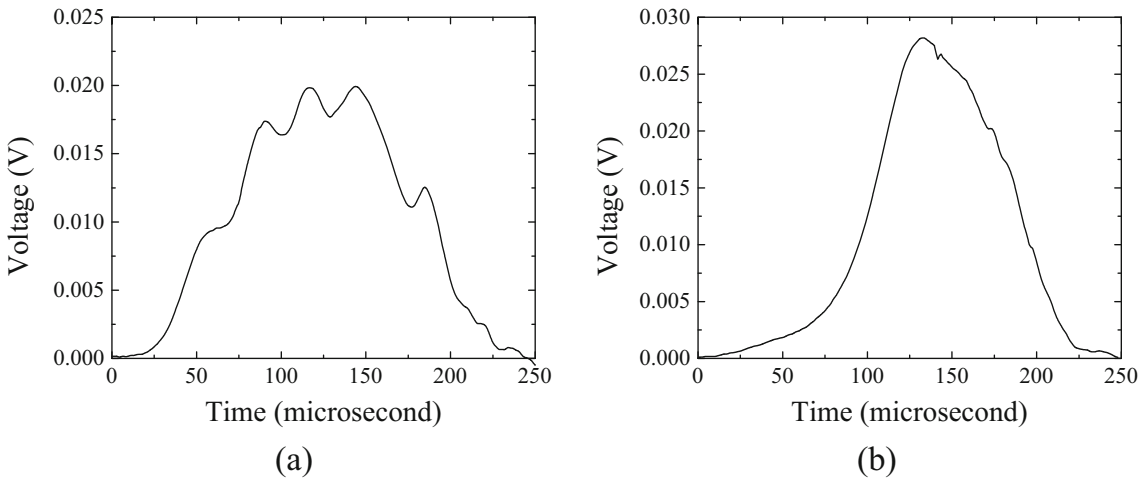

Fig. 3 Typical incident waveforms using the 50.8 mm Kolsky compression bar arrangement: (**a**) 25.4 mm diameter x 1.5 mm thick solid copper pulse shaper; (**b**) 9.0 mm diameter x 1.5 mm thick solid copper pulse shaper

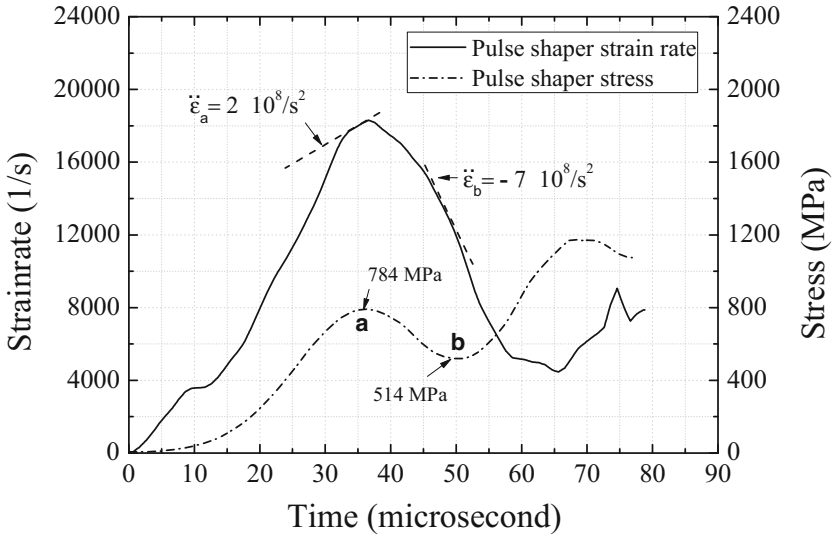

Fig. 4 Stress and strain-rate histories for a 25.4 mm diameter and 1.50 mm thick copper specimen using the 50.8 mm compression Kolsky bar with no pulse shaping

second source comes from large specimen deformation. When the specimen deformation becomes sufficiently large the radial expansion rate continues to increase despite being in a state of constant axial strain-rate to satisfy volume conservation. The explicit impact of inertia effects on experimental results for soft materials was observed by Song et al. [46, 47]. More recently, Warren and Forrestal [49] proposed a closed-form analytical solution to estimate the inertia-induced pressure in incompressible solid disk specimens. The analytical solution of Warren and Forrestal is given as,

$$\overline{p} = \frac{\rho a_0^2}{8(1-\varepsilon_x)^2}\ddot{\varepsilon}_x + \frac{3\rho a_0^2}{16(1-\varepsilon_x)^3}\dot{\varepsilon}_x^2 \tag{3}$$

where $\overline{p}$ is the inertia-induced pressure (in the axial and radial directions), ρ is density, a_0 is the initial radius of the solid disk specimen, ε_x the specimen axial engineering strain, while $\dot{\varepsilon}_x$ and $\ddot{\varepsilon}_x$ are the specimen axial strain-rate and axial strain-rate acceleration, respectively. The first term in equation 3 describes the inertia induced by the strain-rate acceleration, $\ddot{\varepsilon}_x$, in the specimen; this term usually reduces to zero once the specimen deformation has reached a constant strain-rate ($\ddot{\varepsilon}_x = 0$). The second term in equation 3 is a function of strain-rate, $\dot{\varepsilon}_x$, and strain, ε_x, and increases rapidly with accumulation of specimen strain even at constant strain-rate. It is straight forward from equation 3 that the inertial stress is a function of specimen strain, strain-rate, and strain-rate acceleration; however, it remains to be seen if the inertia-induced pressure, $\overline{p}$, caused the stress variation in the transmitted wave (i.e., specimen stress). To assess the inertia-induced pressure the inertial stress at the peaks (points a and b in Fig. 4) in the stress profile were calculated and compared. Given ρ = 9,000 kg/m^3 and a_0 = 12.5 mm for the solid copper disk specimen and other parameters as indicated in Fig. 4, the calculated difference in $\overline{p}$ is approximately −444 MPa between points a and b. The negative sign indicates the inertia-induced axial stress has decreased between these two states, which qualitatively agrees with the decline of both $\dot{\varepsilon}_x$ and $\ddot{\varepsilon}_x$ in the stress history curve from points a to b.

Note that the actual stress decrease measured from the curve yields a value of 270 MPa, which is smaller than the analytical results. An explanation for this difference is that while the copper disk specimen deforms from point a to b the plastic strain increases from approximately 0.28 to 0.51. It is the authors' view that the specimen stress accumulated from strain hardening has compensated for part of the pressure drop and resulting in a reduced net axial stress decrease as measured by the strain gages.

Annulus Pulse Shapers

Previous studies on high-rate compression testing of soft materials revealed similar radial inertia effects for solid disk specimens [46, 47]. The distribution of this inertia pressure within the specimen follows a parabolic function along the diameter. The pressure is highest at the specimen center while at the circumference the pressure becomes zero due to a stress-free boundary condition. Researchers have created the same stress-free boundary condition at the specimen center by fabricating annular-type specimens that substantially reduce the amplitude of the inertial pressure [47]. Later work has shown that the residual inertia in the annular specimens still overwhelms the intrinsic material response for most soft specimens [37]. In the present work, the authors adopt this concept and extend the use of an annular geometry to pulse shaper design for large-diameter Kolsky bars. This allowed the authors to significantly limit inertial pressure to negligible levels in comparison with the intrinsic response of the pulse shaper material. Equation 3 substantiates this argument since inertial pressure also exists in small-diameter solid copper pulse shapers, however, the magnitude of this pressure is not high

enough to induce oscillations within the incident wave. Based on the annular concept an 14.4 mm diameter central hole was introduced in the 25.4 mm diameter solid copper pulse shaper. Following proper calibration of the striker velocity, an almost linear incident wave, free of oscillations, was produced as shown in Fig. 5.

In theory, similar pressure reduction could also be achieved by using multiple small-diameter solid copper pulse shapers that have an equivalent cross-sectional area to the annular pulse shaper. From a practical standpoint, placing multiple evenly spaced small pulse shapers on the impact end of the incident bar is a tedious and challenging task. Several difficulties may arise: (1) ensuring uniform contact between the striker and each small solid pulse shaper during impact and (2) avoiding contact and interference between the neighboring small solid pulse shapers during the deformation process. If either of these situations occurs the quality of the incident wave will be compromised. Therefore, the annular pulse shaper design offers an effective solution for significant reduction of the radial inertia effects while avoiding any of the aforementioned problems. It is believed that this technique has great potential and is worth exploring for large-diameter Kolsky bar experiments on a variety of materials and structures.

Results and Discussion

Mechanical Response of Concrete at High Rates

The effectiveness of the annular pulse shaper design was examined through Kolsky bar compression experiments on SCHSC specimens at two strain-rates. As previously mentioned, maintaining dynamic stress equilibrium and constant strain-rate deformation in the specimen are the two primary boundary conditions determining the validity of Kolsky bar experiments. When characterizing brittle materials, these boundary conditions are particularly important because the total specimen deformation prior to failure is very small (≤1.0 %). Consequently, these boundary conditions are required to be satisfied within a short period of time (typically less than 50 μs). To satisfy these boundary conditions in all experiments for this research annular pulse shapers were designed for strain-rates of 240 s^{-1} and 100 s^{-1}. Experiments at 100 s^{-1} strain-rate used six small additional solid pulse shapers mounted on top of the annular pulse shaper to further decrease the strain-rate acceleration and avoid large fluctuations in strain-rate prior to reaching the desired constant rate of 100 s^{-1}. The testing conditions for all experiments are presented in Table 4 while photographs of the fabricated annular pulse shapers mounted on the impact end of the incident bar are shown in Fig. 6.

To demonstrate the effectiveness of the annular pulse shaper concept, raw experimental data is presented in Fig. 7 for 100 s^{-1} and 240 s^{-1} strain-rates. In Fig. 7, plateaus are evident in the reflected waves indicating the specimens achieved constant strain-rate deformation prior to failure as indicated by the sharp increase in the strain-rate profile. In general, the total specimen deformation time prior to failure (up to the end of the constant strain-rate region) increases from 60 to 140 μs as the strain-rate decreases from 240 s^{-1} to 100 s^{-1}. Thus, the duration of constant strain-rate prior to failure is longer for the strain-rate of 100 s^{-1}.

According to one-dimensional wave theory for Kolsky bar experiments, the stress at front (incident bar side) and back (transmission bar side) surfaces of the specimen can be calculated as

$$\sigma_F = \frac{A_b}{A_s} E_b(\varepsilon_i + \varepsilon_r), \tag{4}$$

$$\sigma_B = \frac{A_b}{A_s} E_b(\varepsilon_t) \tag{5}$$

where σ_F and σ_B are the specimen stress on the front and back surfaces of the specimen, respectively. In equations 4 and 5, A_b and A_s are the cross-sectional areas of the Kolsky bar and specimen, respectively, while again ε_i, ε_r and ε_t are the strains

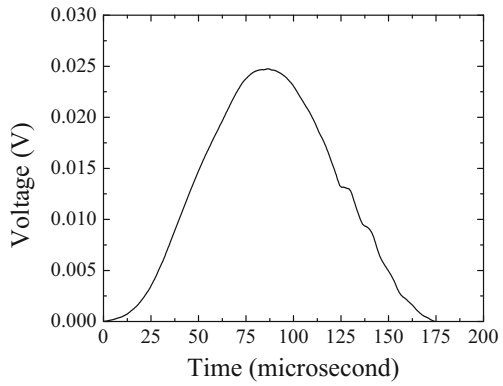

Fig. 5 Linear incident wave generated using an annular copper pulse shaper (O.D. = 25.4 mm, I.D. = 14.4 mm). Note that compared to Fig. 3(a) the inertia induced oscillations are eliminated

Table 4 Testing conditions for SCHSC specimens

Strain Rate (1/s)	Solid O. D. (mm)	Pulse shaper Thickness (mm)	Annular O. D. (mm)	Pulse I.D. (mm)	Shapers Thickness (mm)
100	3.20	0.51	25.4	15.9	1.00
240	–	–	25.4	14.4	0.80

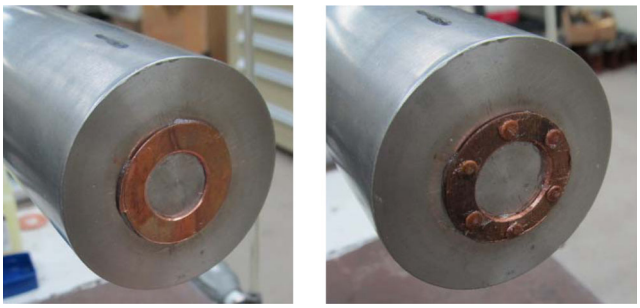

Fig. 6 Photographs of the pulse shaper designs used in all experiments: (**a**) 240 s^{-1} copper pulse shaper; (**b**) 100 s^{-1} copper pulse shaper

associated with incident, reflected, and transmitted waves, respectively. Using equations 4 and 5 with the experimentally collected incident, reflected, and transmitted wave signals the dynamic stress histories of the concrete specimens can be calculated and compared to assess stress equilibrium. Figure 8 presents the stress equilibrium for a single experiment conducted at 240 s^{-1} strain-rate. The stress at the front and back of the specimen are in good agreement indicating the concrete specimen was under stress equilibrium during the dynamic deformation process.

It is well understood that concrete is heterogeneous and requires multiple experiments at a single strain-rate to adequately account for such heterogeneity. For this reason, five experiments were conducted at each strain-rate using well-controlled loading conditions through the pulse shaping technique. The repeatability of the loading conditions (i.e., incident wave) is shown in Fig. 9.

The mechanical response for all experiments was determined by using the measured bar signals and equations 1 and 2. The dynamic stress-strain response is summarized in Fig. 10 and superposed with the quasi-static results obtained with a strain-rate of 10^{-4} s^{-1}. Figure 10 indicates a

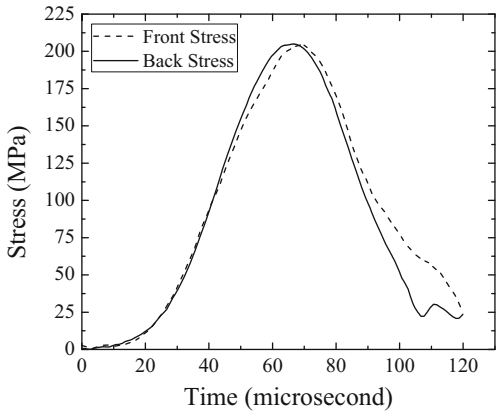

Fig. 8 Dynamic stress equilibrium for 240 s^{-1} strain-rate

strong rate dependency in failure strength at a strain-rate of 240 s^{-1} showing a maximum compressive strength of 220 MPa. This is approximately three times stronger than the quasi-static compressive strength. It is also noted that over the Kolsky bar strain-rate regime (100 s^{-1} to 240 s^{-1}), the compressive strength increased by 20 %. The strain-rate sensitivity for the material investigated in this study is presented in Fig. 11.

The elastic modulus, however, does not exhibit noticeable strain-rate sensitivity other than minor variations between specimens due to the material heterogeneity. One unique feature of the dynamic mechanical response obtained in this study is that the specimens' stresses do not (immediately) drop to zero following peak stress indicating the possibility of fragmentation and progressive failure. These results are in agreement with previous work on the dynamic compressive response of pure mortar [27]. Grote et al. revealed that the pure mortar did not exhibit strain-rate sensitivity until after 290 s^{-1}, whereas in this study, the strength of the SCHSC specimens increased three fold (see Fig. 11) at about the same strain-rate. In general, the dynamic response of SCHSC showed a similar

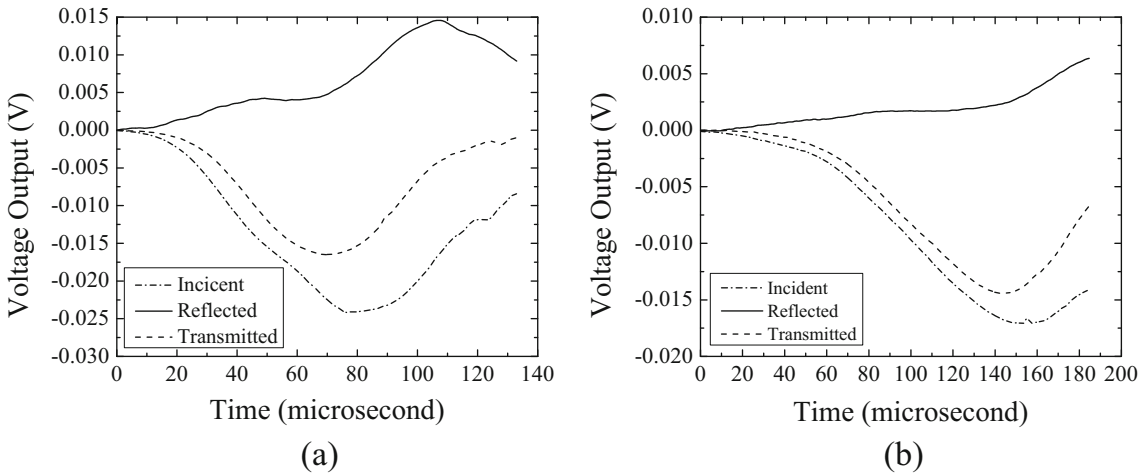

Fig. 7 Original Kolsky *bar* waveforms: (**a**) 240 s^{-1}; (**b**) 100 s^{-1}

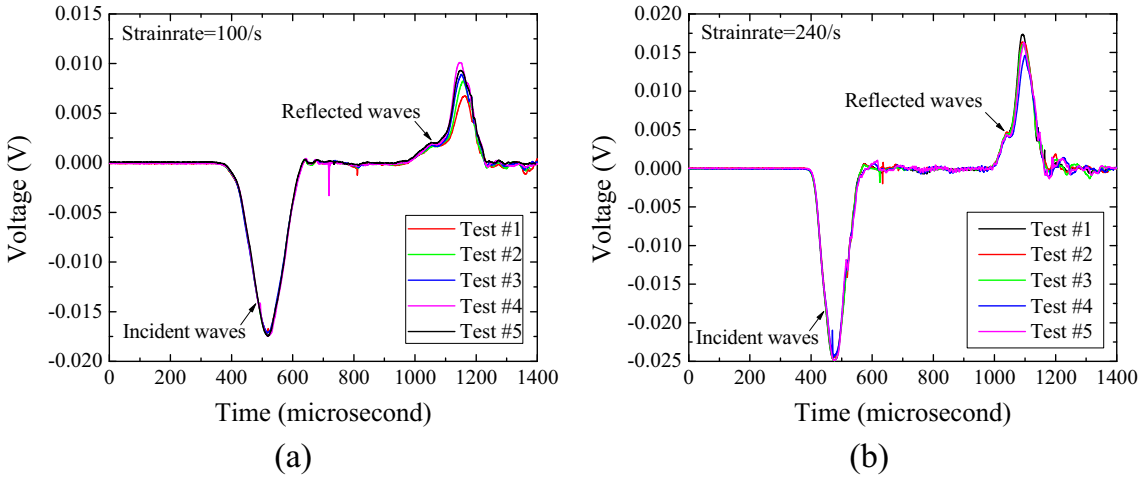

Fig. 9 Repeatability of well controlled loading conditions: (**a**) 100 s^{-1}; (**b**) 240 s^{-1}

trend in strain-rate dependency as reported by others for concrete materials in compression [27, 33, 41, 43] and tension [9, 19, 31, 48].

The primary goal of this study was not to further populate the dynamic concrete data within the literature that has been made available to the research community over the past decades. The authors' intention was focused on establishing a reliable large-diameter Kolsky compression bar experimental technique that may be used for future concrete materials (or other geo-materials) research, especially when large-size specimens are of importance. It is clearly shown (see Figs. 7, 8, and 9) that the carefully designed annular pulse shapers provide repeatable testing conditions for specimens (e.g., constant strain-rate and dynamic stress equilibrium) that are strictly satisfied to warrant valid experimental results. In addition to the primary objective of the research, it is evident that the new loading technique successfully characterizes the dynamic mechanical response of the SCHSC material investigated. The dynamic data in Fig. 11 shows small variations in the compressive strength for both 100 s^{-1} and 240 s^{-1} strain-rates. This small variation is due to the repeatability of the loading technique and minimization of the variation in the specimen strain-rate from test to test. Consequently, optimum repeatability for the specimen compressive strength could be realized. The ability to minimize these variations is very important when interpreting the mechanical properties of concretes due to their highly rate-sensitive nature and heterogeneity.

Effect of Specimen Inertia

Equation 3 suggests that the inertia induced pressure in any deformable solid is strongly dependent upon the specimen

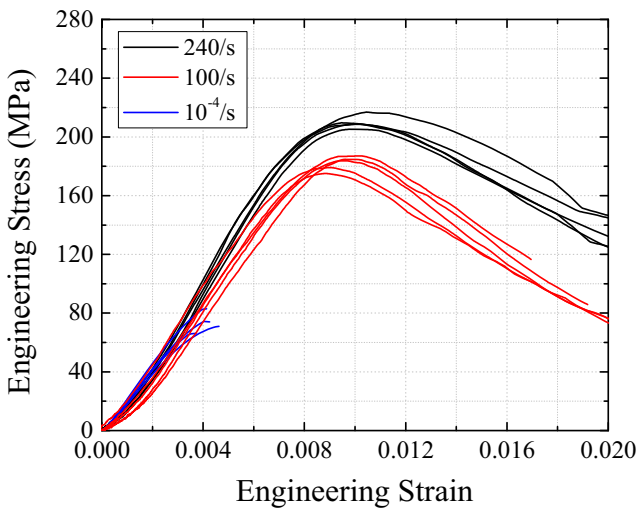

Fig. 10 Engineering stress-strain response of SCHSC under varying strain-rates

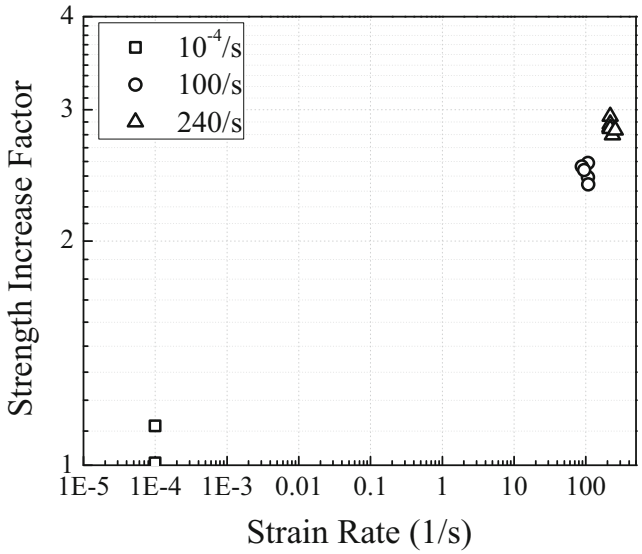

Fig. 11 Strength Increase Factor as a function of strain-rate for SCHSC concrete

radius a_0. As the diameter of the concrete specimen increases, the inertia may impose additional stresses in both the radial and axial directions. Pressure dependencies in concrete due to radial confinement is well understood indicating that the imposed radial inertia may play an important role in evaluating the failure strength enhancement, and therefore needs to be carefully investigated along with data interpretation. Li and Meng [32] studied this possible effect on concrete-like brittle materials through numerical simulations. Later work by Forrestal et al. [21] presented a set of analytical solutions regarding specimen radial inertia and are given as

$$\sigma_r = \frac{\nu(3-2\nu)}{8(1-\nu)}\left(a_0^2 - r^2\right)\rho\ddot{\varepsilon}_x, \tag{6}$$

$$\sigma_x = \frac{\nu^2(3-2\nu)}{4(1-\nu)}\left[a_0^2 - \frac{2r^2}{(3-2\nu)}\right]\rho\ddot{\varepsilon}_x, \tag{7}$$

where σ_r and σ_x are the inertia-induced radial and axial stresses at location r (the radial distance from specimen center), respectively, and ν is the specimen Poisson's Ratio.

It should be noted that although equations 6 and 7 share certain similarities with equation 3, equation 3 was derived to approximate the inertial stress for materials that exhibit large deformations, such as copper pulse shapers. However, for brittle materials such as concretes, the deformation is typically small (≤1 %). To account for the brittleness of concretes, Warren and Forrestal [49] derived equations 6 and 7 to neglect inertia imposed by large deformations. Therefore, equations 6 and 7 consider elastic deformation for which the material is compressible (ν<0.5) while equation 3 considers the material as incompressible (ν=0.5). Note, that the confining pressure, σ_r, is maximum at the specimen center and decreases to zero at the specimen circumference.

The axial inertia, σ_x, also varies with location with the integral of σ_x over the entire specimen cross-sectional area yielding the average of the additional axial stress imposed by inertia. This additional stress is superposed onto the intrinsic material response measured by the strain gages. To make a conservative estimation of the inertia effect, it was assumed ν=0.5 with an average specimen density of 2,150 kg/m^3 and specimen radius of 25.4 mm. The estimation of strain-rate acceleration, $\ddot{\varepsilon}$, is determined using the specimen strain-rate history as presented in Fig. 12.

Figure 12 indicates that the strain-rate acceleration, $\ddot{\varepsilon}$, is largest during the initial ramp up stage. Once the specimen deformation reaches constant strain-rate the strain-rate acceleration, $\ddot{\varepsilon}$, becomes zero. In the early stage of deformation the strain-rate changes significantly and $\ddot{\varepsilon} = 7.35\text{x}10^6 s^{-2}$. Substituting this value of strain-rate acceleration into equations 6 and 7 and integrating σ_x over the cross-sectional area, the specimen inertia stress is determined to be,

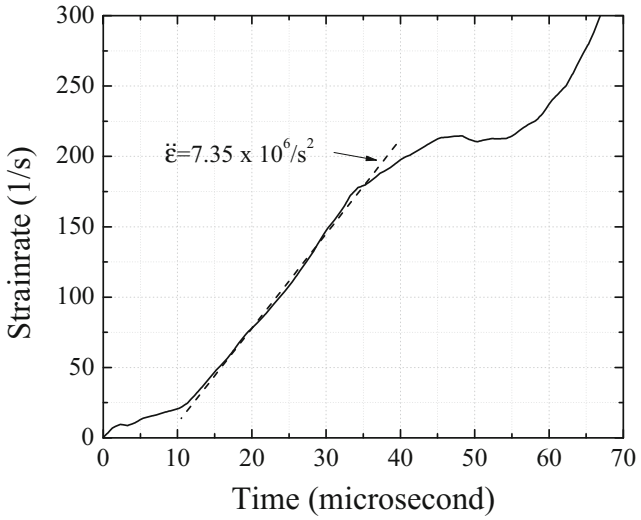

Fig. 12 Typical specimen strain-rate history for SCHSC specimens for 240 s^{-1} (*solid line*) with the indicated specimen strain-rate acceleration (*dotted line*)

$$\sigma_{r=0} = 0.6\text{MPa}, \quad \int \sigma_x dA = 0.3\text{MPa}$$

These low values verify that the inertia-induced confining pressure and axial stresses are minimal prior to the start of specimen fracture. Furthermore, at the specimen center where the radial confinement, σ_r, is greatest, the magnitude of the confining pressure is only 0.6 MPa. This low confining pressure is small and does not induce any noticeable enhancement to the material's compressive strength. Compared to the average dynamic compressive strength of 200 MPa, the additional axial stress induced by inertia (0.3 MPa) is small enough that it can be safely neglected from the specimen's stress history. It should be noted, that even though the magnitude of inertial stress for concrete specimens is case sensitive which may vary with material type and/or testing conditions, it is reasonable to conclude that for Kolsky bar experiments with specimen diameters up to 50.8 mm the inertia in specimens may not play a critical role in compressive strength enhancement. This conclusion is further reinforced for brittle materials like concrete since the maximum achievable constant strain-rate and strain-rate acceleration in Kolsky bar experiments are limited [39]. These very low initial values (<1 MPa) of inertia-induced stress suggest that the inertia stress signal is likely to reside within a range that is comparable to the experimental noise.

Conclusions

The primary objective of this study was to develop a viable pulse shaping technique for large-diameter Kolsky bar

experiments for concrete materials. Previous pulse shaping techniques for brittle materials were established with smaller diameter bars that use smaller pulse shapers. As the size of the Kolsky bar and pulse shaper drastically increase to accommodate larger concrete specimen diameters, radial inertia in the pulse shaper becomes non-negligible and interferes with the intrinsic pulse shaper material response during deformation. The inertia-induced stress significantly influences the incident wave which would otherwise exhibit a linear ramp. The present study has shown that by implementing an annular pulse shaper geometry for large-size pulse shapers the radial inertia effects can be attenuated sufficiently to not influence the incident wave. In other words, a linear wave, which is desired for Kolsky bar experiments on brittle materials, was realized through this modified pulse shaping technique. The validity of this concept was examined through testing a SCHSC material using a 50.8 mm diameter Kolsky compression bar located in the High-Pressure Particulate Physics (HP3) facility at the U.S. Air Force Research Laboratory, Eglin AFB, FL. The experimental results showed that with proper design of the annular shaper the concrete specimens deformed under dynamic stress equilibrium and constant strain-rate until failure occurred. All testing conditions were well controlled for both investigated strain-rates (100 s^{-1} and 240 s^{-1}) with minimal observed scatter in strain-rate and failure strength. An additional uncertainty associated with a large diameter Kolsky bar is the possible inertial effects in the specimens that may result in artificial enhancement to the failure strength under uniaxial stress loading conditions. Through the comparison of analytical model predictions and experimental results it is shown that, for high strength concrete materials, the inertia-induced stress is almost negligible compared to the intrinsic strength of the material. The loading technique developed in this study shows great promise and can be successfully applied to characterize the dynamic response of other geomaterials on large Kolsky bars.

References

1. Albertini C, Cadoni E, Labibes K (1999) Study of the mechanical properties of plain concrete under dynamic loading. Exp Mech 39: 137–141
2. ASTM-C150 (2011) Standard specification for Portland cement. ASTM International, West Conshohocken
3. ASTM-C989 (2007) Standard practice for making and curing concrete test specimens in the laboratory. ASTM International, West Conshohocken
4. ASTM-C989 (2012) Standard specification for coal Fly Ash and Raw or calcined natural pozzolan for Use in concrete. ASTM International, West Conshohocken
5. ASTM-C989 (2012) Standard specification for slag cement for use in concrete and mortars. ASTM International, West Conshohocken
6. Bischoff P, Perry S (1991) Compressive behavior of concrete at high strain rates. Mater Struct 24:425–450
7. Bischoff P, Perry S (1995) Impact behavior of plain concrete loaded in uniaxial compression. J Eng Mech 121:685–693
8. Brace WF, Jones AH (1971) Comparison of uniaxial deformation in shock and static loading of three rocks. J Geophys Res 76:4913–4921
9. Brara A, Klepaczko JR (2006) Experimental characterization of concrete in dynamic tension. Mech Mater 38:253–267
10. Cadoni E, Solomos G, Albertini C (2009) Mechanical characterization of concrete in tension and compression at high strain rate using a modified hopkinson bar. Mag Concr Res 61:221–230
11. Chen W, Lou H (2003) Dynamic compressive testing of intact and damaged ceramics. Ceram Eng Sci Proc 24:411–416
12. Chen W, Lou H (2004) Dynamic compressive responses of intact and damaged ceramics from a single split hopkinson pressure bar experiment. Exp Mech 44:295–299
13. Christensen RJ, Swanson SR, Brown WS (1972) Split-hopkinson-bar tests on rock under confining pressure. Exp Mech 12(11):508–513
14. Davies EDH, Hunter SC (1963) The dynamic compression testing of solids by the method of the split hopkinson pressure bar. Journal of Mechanics and Physics of Solids 11:155–179
15. Dharan CKH, Hauser FE (1970) Determination of stress–strain characteristics at very high strain rates. Exp Mech 10:370–376
16. Donze F, Magnier S, Daudeville L, Mariotti C, Davenne L (1999) Numerical study of compressive behavior of concrete at high strain rates. J Eng Mech 125:1154–1163
17. Duffy J, Campbell JD, Hawley RH (1971) On the use of a torsional split hopkinson bar to study rate effects in 1100–0 aluminum. ASME Trans J Appl Mech 37:83–91
18. Ellwood S, Griffiths LJ, Parry DJ (1982) Materials testing at high constant strain tates. J Phys E Sci Instrum 15(3):280–282
19. Erzar B, Forquin P (2010) An experimental method to determine the tensile strength of concrete at high rates of strain. Exp Mech 50:941–955
20. Field JE, Walley SM, Proud WG, Goldrein HT, Siviour CR (2004) Review of experimental techniques for high rate deformation and shock studies. International Journal of Impact Engineering 30:725–775
21. Forrestal MJ, Wright TW, Chen W (2007) The effect of radial inertia on brittle samples during the split hopkinson pressure bar test. International Journal of Impact Engineering 34:405–411
22. Frantz C, Follansbee P, Wright W (1984) Experimental techniques with the split hopkinson pressure bar. In: Proceedings of the 8th International Conference on High Energy Rate Fabrication, Pressure Vessel and Piping Division, ASME, Texas, TX
23. Frew DJ, Forrestal MJ, Chen W (2001) A split hopkinson bar technique to determine compressive stress–strain data for rock materials. Exp Mech 41:40–46
24. Frew DJ, Forrestal MJ, Chen W (2002) Pulse shaping techniques for testing brittle materials with a split hopkinson pressure bar. Exp Mech 42(1):93–106
25. Gorham D (1989) Specimen inertia in high strain-rate compression. J Phys D Appl Phys 22:1888–1893
26. Gray GT (2000) Classical split-hopkinson pressure bar testing. In: Handbook ASM (ed) Mechanical testing and evaluation, vol 8. American Society for Metals, Materials Park, pp 462–476
27. Grote DL, Park SW, Zhou M (2001) Dynamic behavior of concrete at high strain rates and pressures: I. experimental characterization. International Journal of Impact Engineering 25:869–886
28. Jiao T, Li Y, Ramesh K, Wereszczak A (2004) High rate response and dynamic failure of structural ceramics. International Journal of Applied Ceramics Technology 1:243–253
29. Kim D, Sirijaroonchai K, El-Tawil S, Naaman A (2010) Numerical simulation of the split hopkinson pressure bar test technique for concrete under compression. International Journal of Impact Engineering 37:141–149

30. Kolsky H (1949) An investigation of the mechanical properties of materials at very high rates of loading. Proc R Soc London B62:676–700
31. Lambert DE, Ross CA (2000) Strain rate effects on dynamic fracture and strength. International Journal of Impact Engineering 24:985–998
32. Li Q, Meng H (2003) About the dynamic strength enhancement of concrete-like materials in a split hopkinson pressure bar test. Int J Solids Struct 40:343–360
33. Malvern LE, Jenkens DA, Tianxi T, Ross CA (1985) Dynamic compressive testing of concrete. In: 2nd Symposium on The Interaction of Non-Nuclear Munitions with Structures, Engineering and Services Laboratory - Tyndall AFB, Panama City Beach, FL, pp 194–199
34. Nemat-Nasser S, Deng H (1994) Strain-rate effect on brittle failure in compression. Acta Metallurgica Materialia 42:1013–1024
35. Nemat-Nasser S, Isaacs JB, Starrett JE (1991) Hopkinson techniques for dynamic recovery experiments. Proc R Soc London A435(1894): 371–391
36. Nie X, Chen W, Sun X, Templeton D (2007) Dynamic failure of borosilicate glass under compression/shear loading: Experiments. J Am Ceram Soc 90:2556–2562
37. Nie X, Sanborn B, Weerasooriya T, Chen W (2012) Inertia effects in high-rate compression experiments of soft materials. Proceedings of the Society for Experimental Mechanics, Lombard, pp 123–124
38. Paliwal B, Ramesh K, McCauley J (2006) Direct observation of the dynamic compressive failure of a transparent polycrystalline ceramic (alon). J Am Ceram Soc 89:2128–2133
39. Pan Y, Chen W, Song B (2005) The upper limit of constant strain rate in a split hopkinson pressure bar experiment. Exp Mech 45:440–446
40. Parry DJ, Walker AG, Dixon PR (1995) Hopkinson bar pulse smoothing. Meas Sci Technol 6:443–446
41. Ross CA, Thompson PY, Tedesco JW (1989) Split-hopkinson pressure-bar tests on concrete and mortar in tension and compression. ACI Mater J 86(5):475–481
42. Ross CA, Tedesco JW, Kuennen ST (1995) Effects of strain rate on concrete strength. ACI Mater J 92(1):37–47
43. Ross CA, Jerome DM, Tedesco JW, Hughes ML (1996) Moisture and strain rate effects on concrete strength. ACI Mater J 93(3):293–300
44. Samanta S (1971) Dynamic deformation of aluminum and copper at elevated temperatures. Journal of Mechanics and Physics of Solids 19:117–135
45. Song B, Chen W, Weerasooriya T (2003) Quasi-static and dynamic compressive behavior of a s-2 glass/sc15 composite. Journal of Compositie Materials 37:1723–1743
46. Song B, Chen W, Ge Y, Weerasooriya T (2007) Dynamic and quasi-static compressive response of porcine muscle. J Biomech 40:2999–3005
47. Song B, Ge Y, Chen W, Weerasooriya T (2007) Radial inertial effects in kolsky bar testing of extra-soft specimen. Exp Mech 47:659–670
48. Tedesco JW, Ross CA, Kuennen ST (1993) Experimental and numerical analysis of high-strain rate splitting-tensile tests. ACI Mater J 90:162–169
49. Warren TL, Forrestal MJ (2010) Comments on the effect of radial inertia in the kolsky bar for an incompressible material. Exp Mech 50: 1253–1255
50. Zhang M, Li QM, Huang FL, Wu HJ, Lu YB (2010) Inertia-induced radial confinement in an elastic tubular specimen subjected to axial strain acceleration. International Journal of Impact Engineering 37(4):459–464. doi:10.1016/j.ijimpeng.2009.09.009

DISTRIBUTION LIST
AFRL-RW-EG-TP-2014-005

Defense Technical Information Center Attn: Acquisition (OCA) 8725 John J. Kingman Road, Ste 0944 Ft Belvoir, VA 22060-6218	1 Electronic Copy (1 File & 1 Format)

EGLIN AFB OFFICES:

AFRL/RWOC (STINFO Office)	1
AFRL/RW CA-N	STINFO Officer Provides Notice of Publication
AFRL/RWML (Attn: Martin Schmidt)	1